Chemistry Africa
https://doi.org/10.1007/s42250-024-01051-9

ORIGINAL ARTICLE

Recovery of Niobium, Titanium and Yttrium from Poly-mineralized Concentrate of Gabal El- Aurf Pegmatitic Rocks, Central Eastern Desert, Egypt

Walid Mahmoud Abdellah[1]

Received: 3 February 2024 / Accepted: 31 July 2024

Abstract
The present study focuses on the processing of a poly-mineralized concentrate attained from a physical beneficiation of process applied to high grade pegmatitic rock sample of Gabal El- Aurf area. The concentrate contains significant amounts of niobium (Nb), tantalum (Ta), titanium (Ti) and rare earth elements (REE) plus yttrium (Y) assaying 19.5, 2.5, 14.2 and 21.2%, respectively. The economic minerals within the concentrate include euxenite, tant-euxenite, samrsakite, allanite, and anatase. The processing procedures involve an alkaline potassium hydroxide fusion applied to the poly- concentrate. This is followed by water leaching to extract dissolved Nb and Ta as water-soluble potassium niobate and tantalate. The remaining hydrous cake undergoes leaching process using 1.2M oxalic acid for selective extraction of titanium as soluble potassium-oxalatotitanat. The residue obtained after oxalic acid leaching is then utilized for the recovery of insoluble REE- oxalate. Subsequently, yttrium is individually separated from a nitrate solution using 2M tri-butyl phosphate (TBP) at pH 1.5. The final proposed technical flowsheet outlines the recovery of pure oxides of Nb–Ta, Ti, and Y.

Keywords El-Aurf · Niobium · Titanium · Yttrium · Fusion · Oxalic acid · TBP

1 Introduction

Gabal (G.) El-Aurf area in the Central Eastern Desert of Egypt is characterized by pegmatitic bodies containing rare metals and radioactive minerals. Positioned between latitudes 26°37 and 26°45S and longitudes 33°20 and 33°26W, the area is geologically classified into South and North pegmatitic bodies [1]. The younger granite of South G. El-Aurf forms a rugged mountain extending about 14 km in the southwest direction, with a triangulation point at 989m above sea level.

The pegmatitic rocks that intrude the monzogranites of G. El-Aurf exhibit poly-phased mineralization, including minerals such as tant-euxenite, euxenite, monazite, bastnasite, anatase, and zircon [2]. These minerals host various rare metals, predominantly REE, Nb, Ta, Ti, and Zr. Two phases of mineralization have been identified: an earlier phase characterized by colorful mineralization with the presence of radioactive minerals like thorite, xenotime, and zircon, and a latter phase characterized by additional accessory minerals (fluorapatite, cassiterite, atacamite, sulfides, and Nb minerals), alongside REE-bearing minerals like pyrochlore and bastnasite, as well as iron oxides minerals [1, 3–5].

Given the significant importance of Nb, Ta, Ti, and REE in modern electronics and nuclear industries, a physical beneficiation process is crucial for extracting these metals from their natural resources [6]. The objectives of physical beneficiation include increasing the metal grade of ore, reducing the amount of associated gangue minerals (quartz, feldspar, hematite, and goethite), lowering leaching plant costs, and enhancing productivity. The beneficiation process typically involves a combination of unit operations such as gravity concentration, magnetic separation, and froth flotation [7–11].

In general, hydrometallurgical processing of Nb–Ta minerals involves acidic and/or alkaline leaching, followed by solvent extraction techniques [12]. The leaching process often employs concentrated acidic solutions, such as HCl/HNO_3/H_2SO_4/H_3PO_4/HCl + HNO_3, due to the lower solubility of Nb–Ta minerals under mild aqueous conditions [13,

✉ Walid Mahmoud Abdellah
walid_82nma@yahoo.com

[1] Nuclear Materials Authority, El Maadi, P.O. Box 530, Cairo, Egypt

Published online: 17 August 2024

14]. Single HF or a mixture of HF and HNO_3/H_2SO_4 solutions is also effective in dissolving these minerals [15–17]. Alternatively, leaching agents like $NH_4.HF_2$, NaF, and KF can be used, although fluoride leaching systems may face challenges like HF loss through volatilization and wastewater contamination, necessitating treatment [9, 18, 19].

To address these challenges, alternative approaches such as alkaline fusion, roasting followed by water leaching, or a mixture of mineral acid solutions have been employed for the leaching of Ta and Nb from their minerals [20–26]. In the context of titanium leaching, sulfuric acid or hydrochloric acid is commonly employed for extracting titanium from minerals like ilmenite and rutile under optimal leaching conditions, as outlined in studies by Xiong et al.; Haverkamp et al.; Li et al.; Zhao et al.; Nguyen and Lee & Ahn and Lee [12, 27–31]. Organic acids, such as oxalic acid and citric acid, have shown superior leaching efficiencies for extracting metals from inert minerals when compared to mineral acids. The chelation of metal ions by organic ligands contributes to this improved efficiency, as noted by Panda et al.; Miao et al.; & Li et al., [32–34]. Notably, the decomposition of Ti using concentrated KOH followed by organic acids, particularly citric acid and oxalic acid, has been reported to enhance the leaching efficiencies of titanium from potassium titanate roasted material [35–38].

Oxalic acid is distinguished as a more effective leaching agent relative to other organic acids like citric, malonic, and acetic acids. This distinction is based on oxalic acid's unique characteristics, which encompass a higher level of acidity, superior complexing capabilities, and enhanced reduction potential [39, 40]. Studies by Jonglertjunya et al. [41] on the dissolution of ilmenite by oxalic acid reported that 86.4% of Ti was leached under conditions of 4M oxalic acid concentration, 1/20 solid/liquid ratio, and a temperature of 90˚C. In contrast, using the same conditions with 4M sulfuric acid resulted in only 16.1% dissolution of Ti. Also, Nayl and Aly [42] reported on the solubility of Ti and Fe in potassium hydroxide-treated ilmenite using eighty percent oxalic acid. Their findings indicated that the dissolution of titanium (93%) remained unchanged after 180 min., while that of iron (73%) had increased slightly. The extreme dissolution of Ti and Fe was observed with 80% oxalic acid within the studied acid concentration between 20 and 80%. The influence of temperature on the dissolution of ilmenite in oxalic acid was also investigated, revealing a decrease in the percentage of Ti extracted at temperatures higher than 150 °C as result of the hydrolysis of Ti, while the recovery of iron improved with rising temperature.

The significant demand for purified Y compounds in industrial development has led to increased market demand. Solvent extraction (SX) emerges as a widely used commercial technology for Y separation due to its ease of use, scalability, and the ability to achieve high purity in the final product [43]. Various solvents have been employed for the individual separation of Y from other rare earth elements, including Primene JM-T (ω-trimethylalkylamine), di(2-ethylhexyl)phosphoric acid (D_2EHPA), and Tri-butyl phosphate (TBP) [44–46]. Additionally, Cyanex has been utilized for separating Y from light lanthanides [47]. Tri-butyl phosphate has been successfully developed for preparing pure Y_2O_3 from a nitrate solution, as documented in studies by Jorjani and Shahbazi; Li; and Khalil et al. [48–50]

2 Experimental Work

In the investigation of G. El-Aurf area, the raw sample underwent a comprehensive characterization involving mineralogical and chemical specifications, as well as physical beneficiation processes. Subsequent chemical processing steps were applied to the obtained concentrate to recover Nb–Ta oxide, TiO_2, and achieve individual separation of Y_2O_3 from the prepared REE-cake.

2.1 Chemical Characterization

Chemical analyses, encompassing major oxides of both the raw host rock and the concentrated sample, were conducted using Axios advanced WDXRF-PANalytical (Netherlands). The chemical determination of Nb, Ta, and Ti was carried out using the Microwave Plasma Atomic Emission Spectrometer (4200 MP-AES, Agilent Technologies) throughout the entire workflow. Quantitative analysis of REE was performed by UV spectroscopy using Arsenazo III, with Y serving as a reference [51]. The scanning electron microscope (ESEM) equipped with an EDAX microanalysis unit played a crucial role in identifying the final Nb, and REE products, along with some selected mineral grains. Also, Inductively Coupled Plasma (Prism ICP) High Dispersion (Teledyne Leeman Labs. USA) was used for chemical analysis of the final products.

2.2 Mineralogical Characterization

The mineralogical composition of the representative G. El-Aurf rock sample was investigated by initially grinding and sieving it into the grain size range of 1 to + 0.063 mm. Subsequently, the light and heavy fractions were separated using bromoform (sp. gr. 2.84 gm/cm^3). Heavy mineral particles were meticulously picked under a binocular microscope, and selected mineral grains were identified using the X-ray diffraction technique (XRD). A PHILIPS X-ray generator model PW1140/90 fitted with a diffractometer model PW1050/80 was employed. The X-ray tube used was a Cu-target model PW2233/30 fitted with a Ni-filter, operating at 40 kV and 20mA.

2.3 Physical Beneficiation Procedure

A five kg bulk sample from G. El-Aurf raw pegmatitic material underwent a physical upgrading process to concentrate economic minerals and separate them from the gangue one. Initially, the raw material was deslimed to generate a heavy minerals concentrate. The deslimed portion was subsequently segregated using screens with mesh sizes ranging from –1 to + 0.063 mm, a range optimal for gravity-based separation techniques. A laboratory-grade wet Wilfley shaking table (No.13, Germany) was utilized under defined operational parameters: a feed rate of 5 kg/h, water flow of 4 L/min, a stroke length of 10 mm, and a table inclination set at 8 degrees. Following this, the Carpco high-intensity lift-type magnetic separator Model MLH (13) III-5 (USA) was employed to perform magnetic separation. This process successfully separated Nb, Ti, and REE minerals as a magnetic fraction at a current setting of 3A, distinctly apart from the lighter silicate gangue minerals.

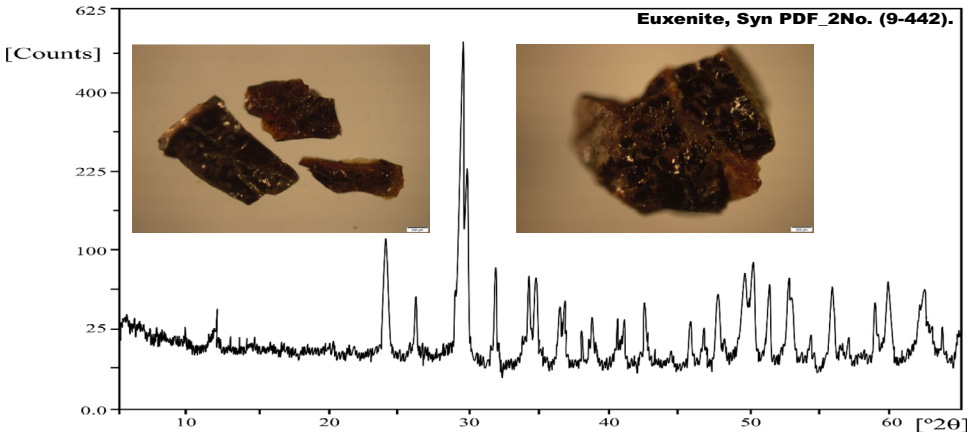

Fig. 1 XRD pattern of brownish euxenite mineral

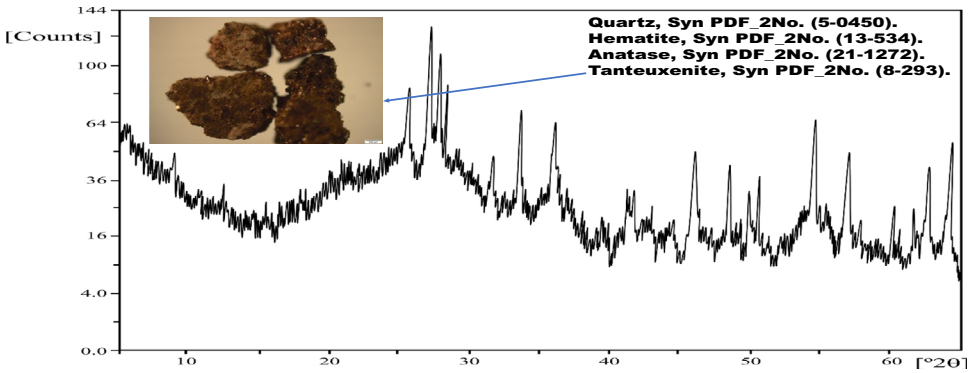

Fig. 2 XRD pattern of tanteuxenite in association with anatase, qurtz and hematite minerals

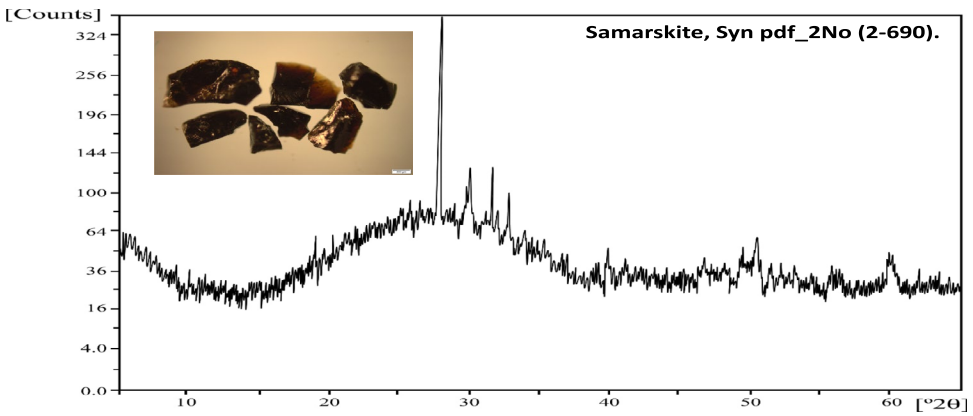

Fig. 3 XRD pattern of samarskite mineral

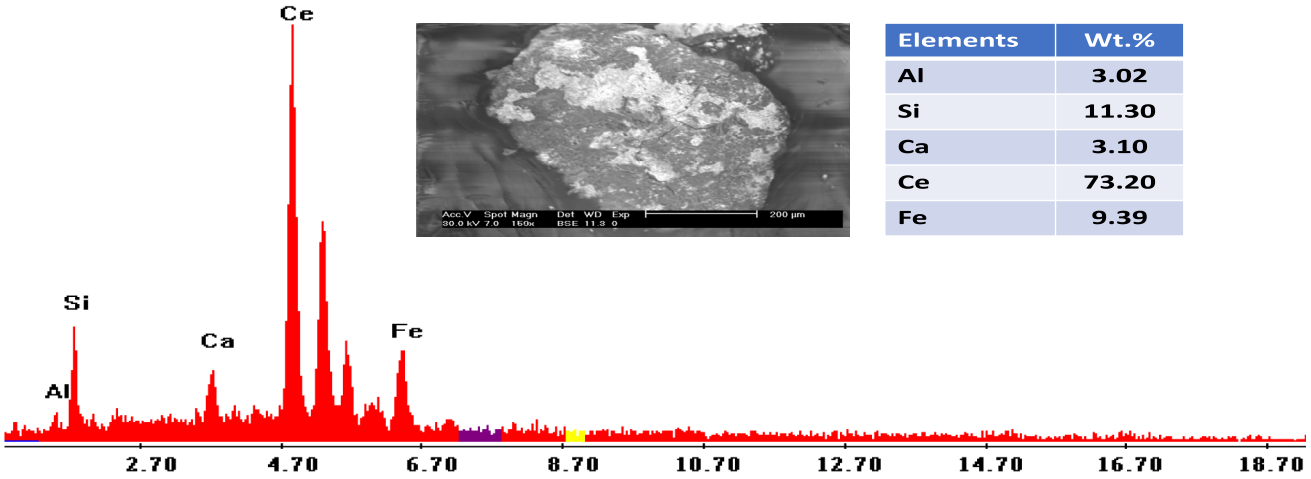

Fig. 4 EDX analysis data of allanite mineral

2.4 Chemical Processing Procedures

Two sequential leaching processes were conducted on the poly-mineralized concentrate sample. The first involved KOH fusion to break down the refractory structure of Nb-Ti and REE minerals, bringing Nb–Ta metal values into a solution. This was followed by atmospheric agitation leaching using oxalic acid to dissolve Ti, leaving the REE as an insoluble oxalate cake. Subsequently, individual separation of yttrium from a nitrate solution was achieved using TBP in kerosene under optimum extraction and stripping conditions.

2.4.1 KOH Fusion of Poly-mineralized Concentrate

A series of experiments were executed, involving the combination of a fixed mass of 5g of finely pulverized concentrate sample (S) with solid KOH (which has a melting point of 360°C) as the fusion reagent (R) in varying proportions (from a 1/1 to a 1/2.5 ratio). This mixture was then subjected to fusion at temperatures ranging from 400 to 600 °C for different time spans (1–2.5 h). Upon cooling, the resultant fused cake (C) was subjected to washing and leaching processes using distilled water at various water to cake (W/C) ratio of 1/10, Leaching time 30 min. The leaching temperature (35–90°C) of the fused cake was also studied to achieve maximum leaching efficiencies of Nb and Ta. After filtration and washing, Nb, Ti, and REE in the prepared alkaline solution were analyzed, and their leaching efficiencies (%) were calculated using the equation:

$$\text{Leaching efficiency, \%} = \frac{\text{Metal concentration in the leach liquor}}{\text{Original metal concentration in the ore}} \times 100$$

The working alkaline leach liquor, essential for Nb and Ta recovery, was prepared by mixing 100g of the working concentrate with KOH under optimum leaching conditions. After filtration and washing with distilled H_2O, the alkaline leach liquor was directed towards Nb–Ta recovery via hydrolysis process.

Table 1 The particle size distribution and amount of heavy minerals in each size fractions

Sieving size	Bulk sample, Wt. (%)	Heavy minerals (g)	Distribution, (%)
– 1 + 0.7 mm	23.2	0.72	22.4
– 0.7 + 0.5 mm	20.5	0.59	18.4
– 0.5 + 0.25 mm	12.6	0.39	12.1
0.25 + 0.125 mm	15.8	0.57	17.8
– 0.125 + 0.063 mm	13.4	0.52	15.6
Sum (– 1 + 0.063mm)	85.5	2.79	86.3
– 0.063 mm	14.5	0.42	13.1
Bulk sample	100	3.21	99.4

2.4.2 Atmospheric Oxalic Acid Agitation Leaching of Spent Residue

The spent residue, containing both Ti and REE along with a small amount of Nb, underwent leaching using an oxalic acid solution. The objective was the selective separation of Ti and Fe from REE, considering various leaching conditions such as oxalic acid concentration (%), solid/liquid (S/L) ratio, leaching time (hour), and leaching temperature (°C). Subsequently, the insoluble REE-oxalate cake, after dissolving Ti, Fe and the remaining Nb, was further processed for individual yttrium separation.

Table 2 Chemical composition of both of the bulk raw sample and the obtained concentrate

Bulk sample	(Wt. %)	Concentrate sample	Wt. (%)
SiO_2	76.9	Nb_2O_5	27.9
Al_2O_3	9.7	TiO_2	23.8
$Fe_2O_3^{tot}$	1.8	Ta_2O_5	3.1
K_2O	3.53	Y_2O_3	18.1
CaO	0.37	RE_2O_3	8.8
MgO	0.7	SiO_2	4.5
Na_2O	1.5	$Fe_2O_3^{tot}$	6.8
MnO	0.29	Al_2O_3	0.9
P_2O_5	0.1	MgO	1.2
TiO_2	0.45	K_2O	0.3
Nb_2O_5	0.75	CaO	1.5
Ta_2O_5	0.05	ZrO_2	0.01
Y_2O_3	0.26	MnO_2	2.1
RE_2O_3	0.11	Na_2O	0.4
ZrO_2	0.2		
*L.O.I	0.6	*L.O.I	0.15

*L.O.I. Loss of Ignition

2.4.3 Individual Separation of Yttrium

The insoluble REE-oxalate cake, post dissolution of Ti, Fe, and the remaining Nb, was employed for the individual separation of yttrium, a predominant element in the cake. To enhance purification, the obtained REE-oxalate, which contained impurities of Mg, Na, and K, underwent dissolution in 10M HCl. Subsequent re-precipitation using NH_4OH at pH 8.5 resulted pure $RE(OH)_3$. The latter was then re-dissolved in a 6M HNO_3 acid solution and directed to a solvent extraction circuit for selective Y extraction. TBP in kerosene, in the presence of a 0.5M ethylenediaminetetraacetic acid (EDTA) solution as a complexing agent, was utilized for this purpose.

3 Results and Discussion

3.1 Mineralogical Characteristics

A crucial objective of this study is to highlight the metallogenic features of the rare metal-bearing pegmatites in G. El-Aurf area. To achieve this, a representative sample, enriched in rare metals like Nb, Ta, Ti, and REE, was selected from extensive sections of the pegmatitic bodies. Mineral grains, representing 3.2% of the heavy fractions, were subjected to XRD and EXD analyses to identify the mineralization.

The data revealed that the principal minerals belong to the Euxenite–Polycrase series. This series is characterized by multiple replacement sites and the presence of Ti, whose content relative to Nb and Ta determines the mineral name. Notably, in euxenite, Nb and Ta are enriched relative to Ti, while in polycrase, Ti is more enriched than Nb and Ta. The identified minerals include:

Euxenite: (Y, Ce, Ca)(Nb, Ta, Ti)$_2$(O)$_6$: widespread niobates resembling columbite-(Fe) and pyrochlore. It exhibits colors ranging from black to greenish or brownish, Fig. 1.

Tant-euxenite: (Y, Ce, Ca)(Ta, Nb, Ti)$_2$(O)$_6$: Named for its similarity to euxenite-(Y) with a higher Ta_2O_5 content than Nb_2O_5. Found in granite pegmatites, it appears brownish-black and is associated with anatase (TiO_2), hematite (Fe_2O_3), and quartz (SiO_2), Fig. 2.

Samarskite: (Y, Ce, Fe^{+3})$_3$(Nb, Ta, Ti)$_5$ O$_{16}$: Dark pitchy to velvety black or dark brown, with irregular massive grains and sub-conchoidal fracture (Fig. 3).

Allanite: Typically black but can be brown or brown-violet. Coated with a yellow–brown alteration product, it comprises various minerals within the allanite group (allanite-(Ce), allanite-(La), allanite-(Nd), and allanite-(Y)), Fig. 4.

This comprehensive mineralogical study of G. El-Aurf raw sample unveiled significant Nb, Ta, Ti, REE, and Zr-bearing minerals alongside gangue minerals like quartz and feldspar. The latter constitutes the main mineral component, emphasizing the need for physical beneficiation before proceeding to recovery processes.

3.2 Gravity Concentration and Magnetic Separation

Depending on the substantial variance in specific gravities of heavy minerals (Sp.gr. 3.9–5.9) in contrast with the associated gangue minerals (primarily quartz and feldspar with Sp. gr. ≈ 2.6), the technique of gravity concentration via a shaking table was harnessed as an effective strategy for the primary separation and concentration of valuable minerals. A 5 kg bulk raw specimen was partitioned into various size fractions (ranging from – 1 to + 0.063 mm), and the Wilfley Shaking Table No. 13 was deployed to procure a preliminary mineral concentrate.

The data in Table 1 revealed variations in specific gravities between heavy minerals and associated gangue minerals. The distribution of heavy minerals among fraction sizes suggested that the crushing operation effectively saved the majority of heavy minerals (86.3%) in fraction sizes (– 1 mm to + 0.063 mm). Approximately 86% of the heavy mineral content accumulated in about 86% of the total weight of the original sample.

The obtained pure concentrate was primarily composed of euxenite, tant-euxenite, samarskite, and anatase associated with zircon. The evident variations in magnetic susceptibilities between Nb-Ti REE minerals and zircon and remains

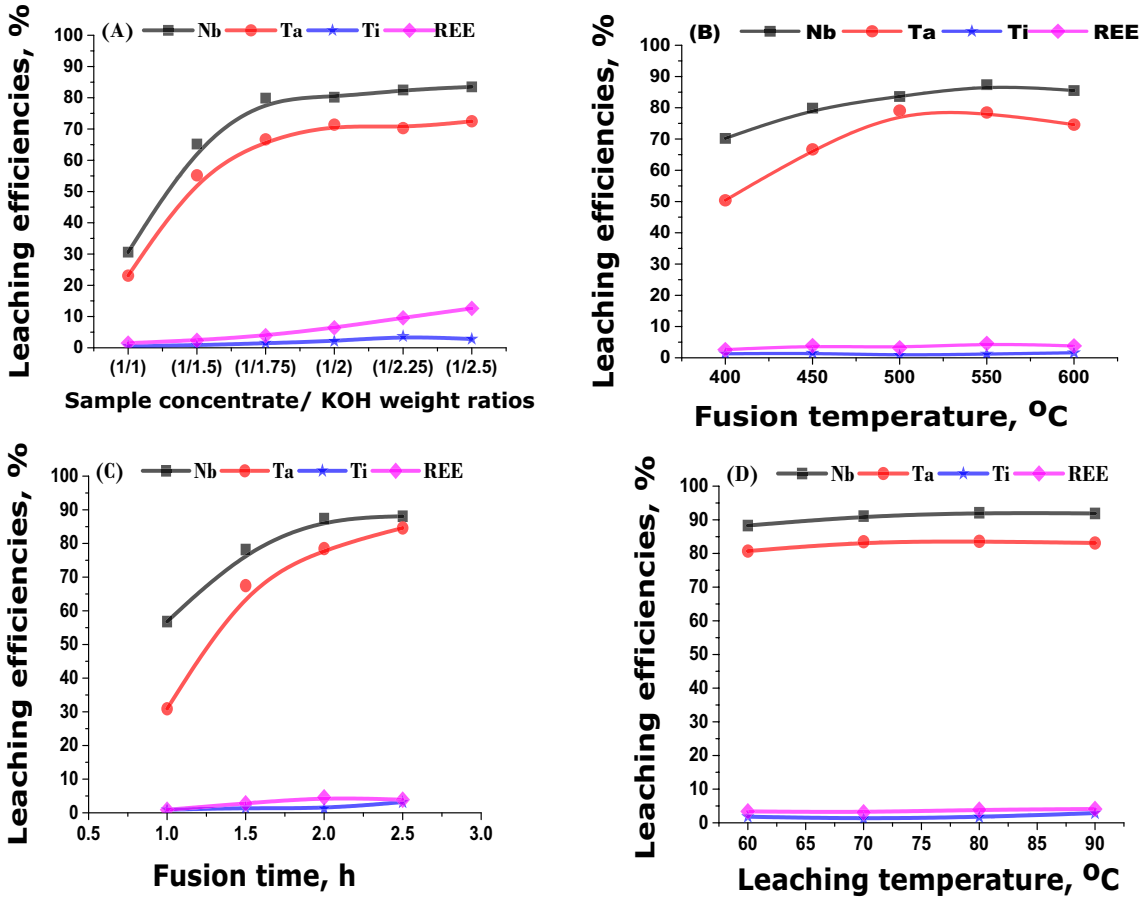

Fig. 5 Effect of sample concentrate/ KOH weight ratio (**A**), fusion temperature (**B**), fusion time (**C**) and leaching temperature (**D**) upon Nb, Ta, Ti and REE leaching efficiencies

silicate minerals formed the basis for their final magnetic separation. A magnetite-free feed was prepared and subjected to magnetic separation using a high-intensity lift-type magnetic separator (Carpco Model MLH (13) III-5). The data illustrated that the ultimate non-magnetic concentrate at 3 amps mainly contained zircon and silicate minerals, while the magnetic concentrate contained tant-euxenite, euxenite, samarskite, and anatase, ready for recovery processes.

3.3 Chemical Composition of the Study Sample

Both the bulk raw sample and the working concentrate of G. El-Aurf underwent chemical analysis for their major and trace element composition (Table 2).The results clearly indicate that the raw material contains economic rare metals such as Nb, Ta, Ti, and REE, alongside Zr. Additionally, it contains well-known gangue minerals, namely quartz and feldspar, evidenced by high SiO_2 (76.9%) and Al_2O_3 (9.7%) content, together with K_2O (3.53%). These findings underscore the importance of applying a physical beneficiation process before chemical treatment to recover the metals of interest. It is noteworthy that after applying the beneficiation process, Nb, Ta, Ti, and (REE + Y) increased from 0.52, 0.04, 0.27, and 0.3% to 19.5, 2.5, 14.2, and 21.2%, respectively. Conversely, SiO_2 content decreased to 4.5% from the original 76.9%, while Al_2O_3 and K_2O decreased to 0.9 and 0.3% from the original 9.7 and 3.53%, respectively.

3.4 Results of KOH Atmospheric Fusion Processes

The mineralogical composition of the working concentrate necessitated the application of alkaline KOH breakdown for the selective leaching of Nb and Ta, separating them from Ti and REE contents. In this process, Nb and Ta were transformed into water-soluble K-niobates and tantalates, while Ti and REE formed an insoluble potassium-hydrous cake. The expected chemical reactions are summarized as follows [20, 52]:

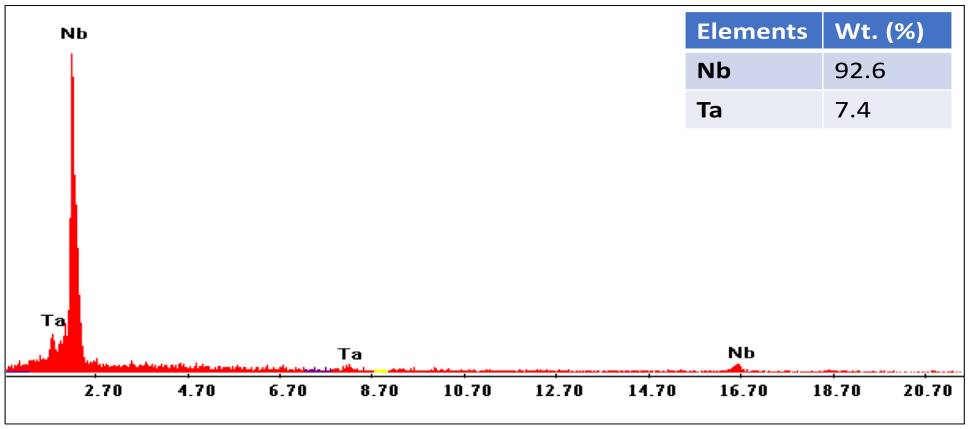

Fig. 6 EXD data of the prepared pure Nb–Ta oxide concentrate

Table 3 Chemical analysis of Ti-REE hydrous cake

Element	Wt.,%	Element	Wt.,%
TiO_2	24.1	Fe_2O_3	6.9
Y_2O_3	17.9	MgO	2.3
RE_2O_3	8.9	CaO	1.1
K_2O	32.1	MnO_2	0.12
Nb_2O_5	1.1	Na_2O	1.0
SiO_2	1.2	moisture	2.4

$$(Fe, Mn)O(Ta, Nb)_2O_5 + 6KOH \rightarrow 2K_3(Ta, Nb)O_4 + (Fe, Mn)O + 3H_2O6K3(Ta, Nb)O_4 + (5 + n)H_2O \rightarrow K_8(Ta, Nb)_6O_{19} \cdot nH_2O + 10KOH4FeO + O_2 \rightarrow 2Fe_2O_3Y_2O_3 + 3KOH \rightarrow Y(OH)_3 + 3K^+3TiO_2 + 4KOH \rightarrow K_4Ti_3O_8 + 2H_2O$$

The relevant factors affecting the leaching efficiencies of the metals of interest were studied as follows:

3.4.1 Effect of Concentrate Sample/KOH Weight Ratio

The effect of varying the weight ratio of concentrate sample to KOH was meticulously analyzed, spanning a range from 1/1 to 1/2.5, while maintaining a consistent set of fusion conditions: a fusion duration of 2 h and a temperature setting of 450°C. Post-fusion, the solidified matrix underwent leaching with distilled water at ambient temperature for a duration of 30 min, adhering to a water to cake (W/C) ratio of 1/10. The findings, depicted in (Fig. 5A), revealed a notable enhancement in the Nb and Ta leaching efficiencies, which escalated from 30.6 and 21.3% to 79.9 and 66.7%, respectively as the weight ratio of concentrate sample to KOH (S/R) was adjusted from 1/1 down to 1/1.75. Nonetheless, a further diminution of the weight ratio beyond 1/1.75 resulted in a marginal increase in Nb and Ta leaching efficiencies. This marginal enhancement may be ascribed to the consumption of KOH for the leaching of interfering metal ions like Si, as discussed by [20].

In contrast, the leaching efficiencies of other economic metal values, namely Ti and REE, remained low, recording values of 1.5 and 3.6%, respectively, at the S/R ratio of 1/1.75.

3.4.2 Effect of Fusion Temperature

The data summarized in Fig. 5B highlighted that the maximum Nb (87.4%) and Ta (78.5%) leaching efficiencies were achieved at 550°C, with an S/R weight ratio of 1/1.75 and a fusion time of 2 h, under fixed leaching conditions (W/C 1/10, 30 min leaching time at room temperature). However, a further increase in fusion temperature up to 600°C resulted in decreased Nb and Ta leaching efficiencies. This decline could be attributed to the fact that the reaction between Nb–Ta and KOH occurred more readily at a temperature of 550°C [20, 25].

3.4.3 Effect of Fusion Time

The impact of fusion time was examined in the range of 1 to 3 h, with the other parameters held constant at a fusion temperature of 550ºC and an S/R weight ratio of 1/1.75, along with W/C 1/10, and a 30 min leaching time at room temperature. The data presented in Fig. 5C revealed that the leaching efficiencies of both of Nb and Ta did not exhibit any improvement beyond 2 h of fusion time. Regarding Ti and REE, their leaching efficiencies remained at very limited values across all fusion time intervals.

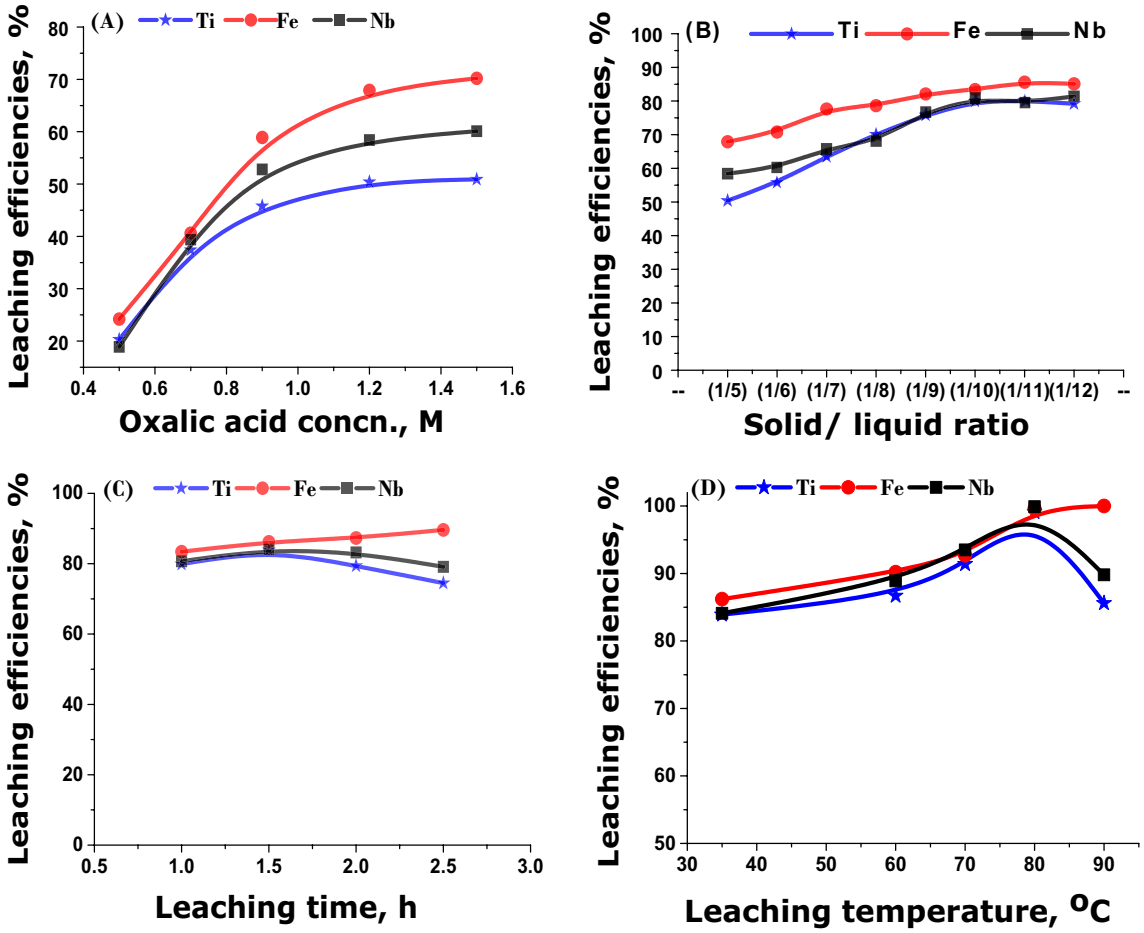

Fig. 7 Effect of oxalic acid conc. (**A**), Solid/ liquid ratio (**B**), leaching time (**C**) and leaching temperature (**D**) upon Ti, Fe and Nb leaching efficiencies

3.4.4 Effect of Water Leaching Temperature

Different water leaching temperatures (ranging from 35 ± 5 to 90°C) for the fused cake were investigated under optimal fusion conditions: S/R weight ratio of 1/1.75, fusion time of 2 h, fusion temperature of 550°C, W/C of 1/10, and leaching time of 30 min. The results indicated that the maximum Nb and Ta leaching efficiencies were achieved at a leaching temperature of 80°C, reaching 91.1 and 83.5%, respectively (Fig. 5D). Conversely, the leaching efficiencies for Ti and REE were limited, recording values of 1.2 and 3.1%, respectively.

3.4.5 Recovery of Nb and Ta

Accordingly, an alkaline pregnant leach liquor of Nb andTa was then prepared by fusing of 100g of the concentrate sample with a solid KOH at the obtained optimum fusion and leaching conditions. The chemical composition of the pregnant solution (1000mL) of pH value 13.2 was found to assay in g/L: 17.8 Nb, 2.1 Ta, 1.3 Si, 0.45 Y and 0.1 Ti. Almost complete precipitation of Nb associated with Ta was achieved via hydrolysis and acidification of the leach liquor (using nitric acid) to pH 2.5 with continuous stirring for 30 min at room temperature to avoid precipitation of the associated impurities e.g. Si and K which remain soluble in the solution. After filtration, washing, drying and ignition at 650°C, the pure Nb–Ta oxide was then identified using EDX analysis (Fig. 6).

3.5 Results of Oxalic Acid Agitation Leaching of Ti-REEs Hydrous Cake

The hydrous cake, left behind after dissolving almost of Nb (91.1%) and 83.5% of Ta, was subjected to XRF analysis to identify its components (Table 3). It was found that the hydrous cake contains significant amounts of the economic elements Ti and REE, accounting for 14.3 and 21.1%, respectively, in addition to the remaining Nb. The concentration of K was notably high at 32.1%, likely due

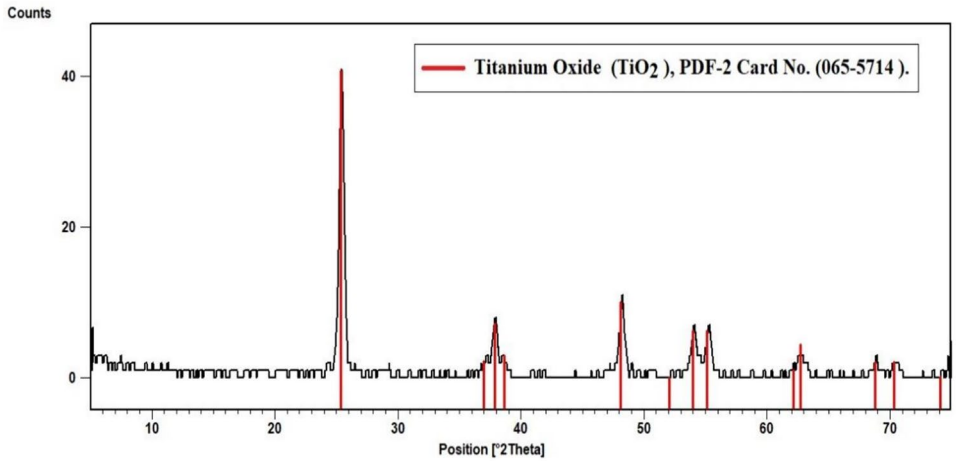

Fig. 8 XRD chart of the prepared pure titanium oxide

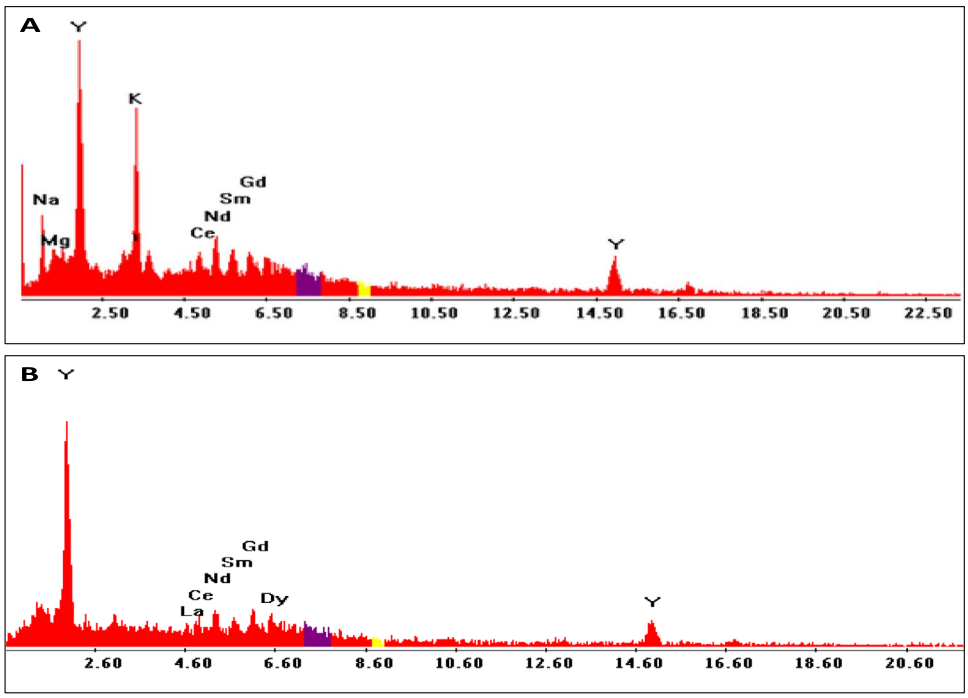

Fig. 9 EDX analysis of impure (**A**) and pure (**B**) REE- cake

to the formation of potassium titantate, hydrous K-REE, and potassium niobate.

To selectively dissolve Ti, an oxalic acid solution was chosen, forming water-soluble potassium-oxalatotitanate (IV) $K_8[TiO(C_2O_4)_2]_4$ [53] and Fe as iron oxalate $Fe(C_2O_4)_3^{3-}$; $Fe(C_2O_4)_2^{2-}$ [54], along with the remaining Nb as niobium oxalates $[Nb(C_2O_4)_2]^-$; $[Nb(C_2O_4)_3]^{3-}$ [55]. The obtained residue after the oxalic acid leaching process was then utilized for the recovery of insoluble REE- oxalate $[REE_2(C_2O_4)_3]$. Various factors affecting the dissolution of metal values, namely Ti, Fe, and Nb, were studied. These factors include oxalic acid concentration, solid/liquid (S/L) ratio, leaching time, and leaching temperature.

3.5.1 Effect of Oxalic Acid Concentration

Different oxalic acid concentrations (ranging from 0.5 to 1.5M) were employed to investigate their impact on the leaching efficiencies of the studied metal values, including Ti, Fe, and Nb, from the potassium hydrous cake. The other leaching conditions were kept constant at room temperature, a leaching time of 1 h, and S/L ratio of 1/5. The results (Fig. 7A) revealed that the leaching efficiencies of all metals of interest increased with the rise in acid concentration, reaching maximum efficiencies of 50.4, 67.9, and 58.4% for Ti, Fe, and Nb, respectively, at 1.2M. Beyond this concentration, a negligible effect on the leaching efficiencies of the metal values was observed.

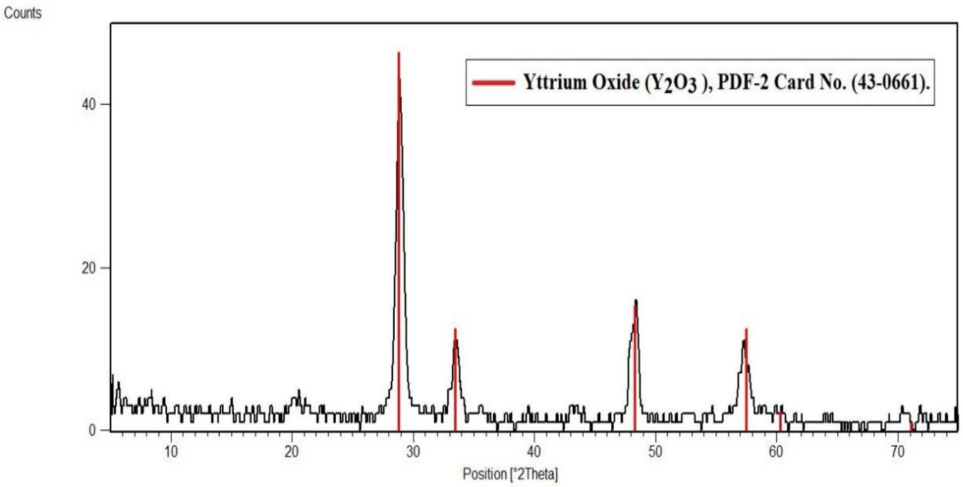

Fig. 10 XRD chart of pure Y oxide cake

3.5.2 Effect of Solid/Liquid Ratio

The impact of the S/L ratio was examined at different ratios ranging from 1/5 to 1/12, using a 1.2M oxalic acid concentration at room temperature and stirring for 1 h. The data (Fig. 7B) demonstrated that the leaching efficiencies of Ti, Fe, and Nb increased with an increasing S/L ratio up to 1/10. However, an S/L ratio higher than 1/10 had no significant effect on the leaching efficiencies of all metal values.

3.5.3 Effect of Leaching Time

Various leaching times, ranging from 1 to 3 h, were considered under the conditions of 1.2M oxalic acid, an S/L ratio of 1/10, and room temperature. The corresponding leaching efficiencies (Fig. 7C) indicated that after 1.5 h, efficiencies of 83.9, 86.2, and 84.1% for Ti, Fe, and Nb, respectively, were achieved. Beyond this time, a slight decrease in the leaching efficiencies of Ti and Nb was observed, possibly due to hydrolysis.

3.5.4 Effect of Leaching Temperature

The influence of leaching temperature on the dissolution efficiencies of various metals was studied across a range from ambient temperature to 90°C, while other leaching parameters were held constant: an acid concentration of 1.2 M oxalic acid, a S/L ratio of 1/10, and a leaching duration of 1.5 h. The collated data (Fig. 7D) underscored that a near-complete dissolution of all target metals was achieved at 80°C. Specifically, at this temperature, dissolution rates of 99.6% for Fe, 99.9% for Nb, and 99.1% for Ti were observed.

Conclusively, based on the oxalic acid agitation leaching experiments conducted on the potassium-Ti, Nb, and REE hydrous cake, it is evident that Ti, Fe, and Nb were predominantly dissolved by oxalic acid, forming water-soluble metal ion oxalates. This process left the REE as an insoluble residue. The following conditions were determined to be optimal: a 1.2M concentration of oxalic acid, a 1/10 S/L ratio, a leaching duration of 1.5 h, and a temperature of 80°C.

3.5.5 Recovery of Titanium

To recover both titanium (Ti) and niobium (Nb), the prepared oxalate leach solution (pH 1.8), containing 29 g/L Ti, 1.1 g/L Nb, 5.2 g/L Fe, and 0.05 g/L Ta, underwent direct precipitation through a hydrolysis process at elevated temperature. Nearly complete precipitation of Ti and Nb was achieved by boiling the oxalate solution, followed by addition to boiled distilled water with stirring for 2 h at 120°C. The Ti-Nb hydrated oxide precipitated and was separated from the soluble Fe-oxalate solution by filtration. The obtained precipitate underwent several washes with water, was dried, ignited at 700°C to produce TiO_2 pigment, and analyzed using XRD (Fig. 8). The ICP chemical analysis of the final product indicated a TiO_2 purity of 97.9% with associated Nb.

3.5.6 Individual Separation of Yttrium

In this procedure, the isolated REE-oxalate cake was retrieved post-filtration, followed by washing and drying at 110°C. It underwent SEM–EDX analysis (Fig. 9A), revealing the presence of trace impurities of K, Mg, and Na within the REE. For enhanced purification, the resultant cake was dissolved in a 10M HCl solution at 85°C and stirred for an hour. Subsequently, re-precipitation was executed using

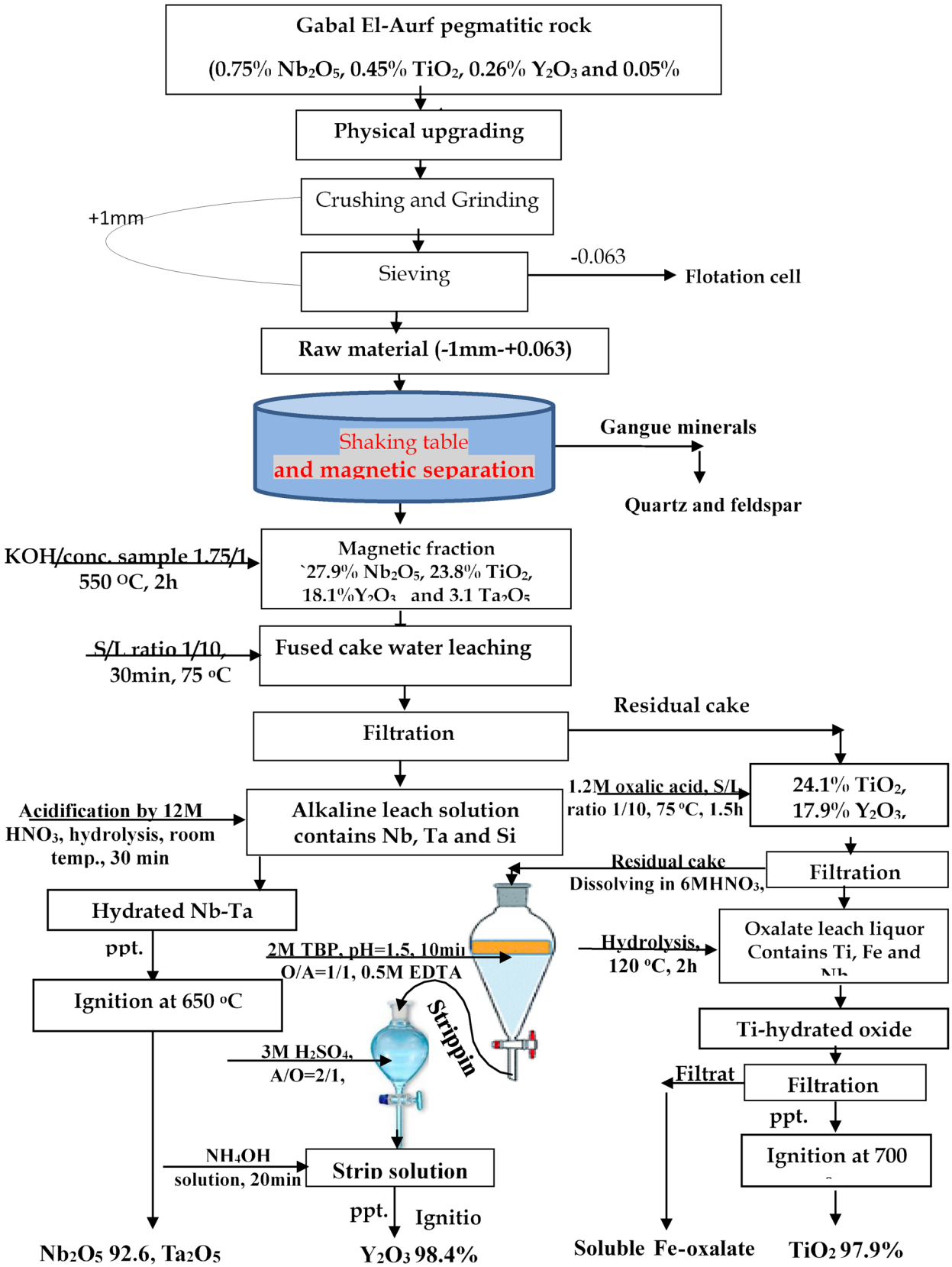

Fig. 11 Proposed techniqual flowsheet for recovering pure Nb–Ta, Ti and Y oxides from G. El-Aurf pegmatitic concentrate

NH_4OH at a pH of 8.5, yielding a highly pure $RE(OH)_3$, as depicted in Fig. 9B [56].

Given yttrium's significant industrial relevance, notably in nuclear energy, metallurgy, ceramics, and luminescence, a dedicated separation process for pure yttrium was initiated. The process commenced with dissolving the REE-hydroxide cake, which assays 53.2% of Y, in a 6M HNO_3 solution to liberate the REE content. The resultant nitrate solution, with a Y concentration of 5.45 g/L, was subjected to a selective extraction process utilizing 2MTBP in kerosene. The process was facilitated by 0.5M EDTA, serving as a complexing agent to sequester various impurities. The incorporation of 0.5M EDTA into the aqueous phase significantly bolstered the selectivity of yttrium separation from other REE. Approximately 90% of Y was extracted from the aqueous phase under specific conditions: using 2M TBP, pH 1.5, and with an O/A ratio of 1/1 over a shaking duration of 10 min. Subsequent water scrubbing (1/1) of the loaded solvent was performed to eliminate any co-extracted REE.

Eventually, around 97% of Y was regenerated from the loaded solvent using 3M H_2SO_4, maintaining an A/O ratio of 2/1 and a shaking time of 20 min. The resultant strip sulfate solution, containing 2.4 g/L of Y, was processed for yttrium precipitation using ammonia solution. This step resulted in the formation of insoluble $Y(OH)_3$ and soluble ammonium sulfate, in accordance with the reaction:

$$Y_2(SO_4)_3 + 6NH_4OH \rightarrow 2Y(OH)_3 + 3(NH_4)_2SO_4$$

Yttrium precipitation was nearly complete at pH of 8.5, with stirring for 20 min at ambient temperature. The yielded Y precipitate was filtered, rinsed with distilled water, dried, and dehydrated to Y_2O_3 at 450°C, as verified through XRD analysis (Fig. 10). ICP chemical analysis of the final product indicated a Y purity of 98.4%, with minor impurities comprising 0.9% Dy and 0.6% Er.

4 Conclusion

The processing methodology for the raw material from G. El-Aurf area is a well-structured and comprehensive approach that involves multiple stages of beneficiation and chemical processing to recover various economic minerals. Initially, the identification of minerals such as tant-euxenite, euxenite, samrsakite, allanite, and anatase sets the foundation. Subsequent concentration techniques, including gravity separation and magnetic separation, efficiently concentrate these economic minerals. The application of an alkaline fusion with KOH, followed by water leaching, proves highly effective in selectively leaching niobium and tantalum as water-soluble potassium niobates and tantalates, achieving remarkable efficiencies of 91.1% and 83.5%, respectively. Furthermore, the use of oxalic acid under optimized conditions enables the dissolution of Ti and Fe from the spent residue. The recovery of hydrated titanium oxide through a hydrolysis process yields a final TiO_2 product with a purity of 97.9%. Additionally, individual separation of Y from the recovered REE oxalate is accomplished using a solvent extraction process with 2M TBP in kerosene and 0.5M EDTA as a chelating agent. The proposed technical flowsheet outlines a systematic approach for the recovery of pure oxides of Nb–Ta, Ti, and Y, highlighting the efficiency and optimization achieved at each step in the complex processing sequence (Fig. 11).

Acknowledgements Deep appreciation and thankful to Prof. T. E. Amer for providing the working sample, critical reading and revising the manuscript. Also, the author is greatly indebted to Prof. Dr. Hanaa Abu Khozeim and Prof. Dr. Mona Fawzy, for their continuous help in accomplishing this work.

Funding Not applicable.

Declarations

Conflict of Interest The author declares no conflicts of interest.

Ethical Approval Not applicable.

Informed Consent Not applicable.

References

1. EL-Sherif AE (2015) Mineralogical and radioactive characterization of Gabal El-Urf Pegmatites, Central Eastern Desert, Egypt. Al-Azhar Bull Sci 26:85–96. https://doi.org/10.21608/absb.2015.22626
2. El Hazek MN, Amer TE, Abu El-Azm MG, Issa RM, Omar SA, El-Hady SM (2009) Characterization and breakdown of South Gabal El A'urf Polymineralized ore material. Eurasian Chem Technol J 35:196–204. https://doi.org/10.18321/ectj309
3. Eliwa H, Breitkreuz C, Khalaf I, El Gameel K (2010) Depositional styles of early Ediacaran terrestrial volcanosedimentary succession in Gebel El Urf area, North Eastern Desert. Egypt J Afr Earth Sci 57:328–344. https://doi.org/10.1016/j.jafrearsci.2009.11.002
4. Khalaf EA, El-Azabi M, Mokhtar H, Bernard K (2020) Stratigraphy and facies architecture of the Neoproterozoic syn- and intereruptive succession: an example from Gabal El Urf, Northeastern Desert, Egypt. Precambrian Res 350:105905. https://doi.org/10.1016/j.precamres.2020.105905
5. El Dabe MM, Ismail AM, Metwaly M (2022) Geology and radioactivity of the Pegmatitic rocks of Gabal El Urf, Northern Eastern Desert Egypt. J Rad And Nucl Appl 7(1):1–13. https://doi.org/10.18576/jrna/070101
6. Williams JC, Boyer RR (2020) Opportunities and issues in the application of titanium alloys for aerospace components. Metals 10:705. https://doi.org/10.3390/met10060705
7. Jordens A, Marion C, Langlois R, Grammatikopoulos T, Rowson NA, Waters KE (2016) Beneficiation of the Nechalacho rare earth deposit. Part 1: gravity and magnetic separation. Miner Eng 99:111–122. https://doi.org/10.1016/j.mineng.2016.04.006

8. Shikika A, Sethurajan M, Muvundja F, Mugumaoderh MC, Gaydardzhiev S (2020) A review on extractive metallurgy of tantalum and niobium. Hydrometallurgy 198:105496. https://doi.org/10.1016/j.hydromet.2020.105496
9. Abdellah WM, Khalafalla MS, Abu Khoziem HA, El Hussaini OM (2021) Physical and chemical processes of Abu Rusheid cataclastic rocks for recovering niobium, zirconium, and uranium compounds. Physicochem Probl Mineral Process 57(5):137–152. https://doi.org/10.37190/ppmp/141585
10. Guo C, Hou S, Jin H, Wang W (2023) Adsorption of tannic acid as depressant in the flotation separation of fluorite and bastnaesite. Mineral Process Extr Metall 132(3–4):172–184. https://doi.org/10.1080/25726641.2023.2243198
11. Nzeh NS, Popoola P, Okanigbe D, Adeosun S, Adeleke A (2023) Physical beneficiation of heavy minerals – part 1: a state of the art literature review on gravity concentration techniques. Heliyon 9(8):e18919. https://doi.org/10.1016/j.heliyon.2023.e18919
12. Nguyen TH, Lee MS (2019) A review on the recovery of titanium dioxide from ilmenite ores by direct leaching technologies. Miner Process Extr Metall Rev 40(4):231–247. https://doi.org/10.1080/08827508.2018.1502668
13. El-Hussaini OM, Mahdy MA (2002) Sulfuric acid leaching of Kab Amiri niobium–tantalum bearing minerals, Central Eastern Desert, Egypt. Hydrometallurgy 64(3):219–229. https://doi.org/10.1016/S0304-386X(02)00045-2
14. Nzeh NS, Adeosun S, Popoola AP, Adeleke A, Okanigbe D (2022) Process applications and challenges in mineral beneficiation and recovery of niobium from ore deposits – a review. Miner Process Extr Metall Rev 43(7):833–864. https://doi.org/10.1080/08827508.2021.1964965
15. Berhe GG, Alberto VR, Tadesse B, Yimam A, Woldetinsae G (2018) Decomposition of the Kenticha mangano-tantalite ore by HF/H_2SO_4 and KOH fusion. Physicochem Probl Mineral Process 54(2):406–414. https://doi.org/10.5277/ppmp1840
16. Allain E, Kanari N, Diot F, Yvon J (2019) Development of a process for the concentration of the strategic tantalum and niobium oxides from tin slags. Miner Eng 134:97–103. https://doi.org/10.1016/j.mineng.2019.01.029
17. Lyu J, Liu Y, Ma Z, Lyu X, Zhou J (2022) Efficient Recovery of niobium and tantalum from ferrocolumbium tantalum by a continuous leaching process using HF − H_2SO_4 − HNO_3 synergistic system. Min Metall Explor 39:1763–1770. https://doi.org/10.1007/s42461-022-00644-7
18. Wu B, Shang H, Wen JK (2015) Sulfuric acid leaching of low-grade refractory tantalum–niobium and associated rare earths minerals in Panxi area of China. Rare Met 34:202–206. https://doi.org/10.1007/s12598-014-0436-7
19. Kabangu MJ, Crouse PL (2012) Separation of niobium and tantalum from Mozambican tantalite by ammonium bifluoride digestion and octanol solvent extraction. Hydrometallurgy 129–130:151–155. https://doi.org/10.1016/j.hydromet.2012.06.008
20. Wang X, Zheng S, Xu H, Zhang Y (2009) Leaching of niobium and tantalum from a low-grade ore using a KOH roast-water leach system. Hydrometallurgy 98:219–223. https://doi.org/10.1016/j.hydromet.2009.05.002
21. Wang XH, Zheng SL, Zu HB, Zhang Y (2010) Dissolution behaviors of Ta_2O_5, Nb_2O_5 and their mixture in KOH and H_2O system. Trans Nonferrous Metals Soc China 20:2006–2011. https://doi.org/10.1016/S1003-6326(09)60409-X
22. - Cardarelli F (2013) Process for upgrading tantalum and niobium ores and concentrates with the recovery of manganese and rare earths oxides. International Application Published Under The Patent Cooperation Treaty (Pct), International Publication Number WO 2013/040694 Al, 28 March 2013.
23. Nguyen TH, Lee MS (2018) A review on the separation of niobium and tantalum by solvent extraction. Miner Process Extr Metall Rev 40(4):265–277. https://doi.org/10.1080/08827508.2018.1526794
24. Wang X, Jia Y, Ma S, Zheng S, Sun Q (2018) Effect of mechanical activation on the leaching kinetics of niobium-bearing mineralisation in KOH hydrothermal system. Hydrometallurgy 181:123–129. https://doi.org/10.1016/j.hydromet.2018.08.012
25. Abdel Wahab GM, Abdellah WM, Yousif AM, Mubark AE (2022) Preparation of pure Nb_2O_5 from Gabal El-Faliq Pegmatite, South Eastern Desert, Egypt. Min Metall Explor 39:833–846. https://doi.org/10.1007/s42461-019-00136-1
26. Habinshuti JB, Munganyinka JP, Adetunji AR, Mishra B, Tanvar H, Mukiza J, Ofori-Sarpong G, Onwualu AP (2022) Caustic potash assisted roasting of the Nigerian ferro-columbite concentrate and guanidine carbonate-induced precipitation: a novel technique for extraction of Nb–Ta mixed-oxides. Results Eng 14:100415. https://doi.org/10.1016/j.rineng.2022.100415
27. Xiong X, Wang Z, Wu F, Li X, Guo H (2013) Preparation of TiO_2 from ilmenite using sulfuric acid decomposition of the titania residue combined with separation of Fe3+ with EDTA during hydrolysis. Adv Powder Technol 24(1):60–67. https://doi.org/10.1016/j.apt.2012.02.002
28. Haverkamp RG, Kruger D, Rajashekar R (2016) The digestion of New Zealand ilmenite by hydrochloric acid. Hydrometallurgy 163:198–203. https://doi.org/10.1016/j.hydromet.2016.04.015
29. Li Z, Wang Z, Li G (2016) Preparation of nano-titanium dioxide from ilmenite using sulfuric acid-decomposition by liquid phase method. Powder Technol 287:256–263. https://doi.org/10.1016/j.powtec.2015.09.008
30. Zhao L, Wang L, Qi T, Chen D, Zhao H, Liu Y, Wang W (2018) Leaching of titanium and silicon from low-grade titanium slag using hydrochloric acid leaching. JOM 70:1985–1990. https://doi.org/10.1007/s11837-018-2929-6
31. Ahn HH, Lee MS (2021) Solvent extraction of Ti(IV) from hydrochloric acid leaching solution of ilmenite. Miner Process Extr Metall Rev 42(5):312–320. https://doi.org/10.1080/08827508.2020.17nn40217
32. Panda S, Costa RB, Shah SS, Mishra S, Bevilaua D, Akcil A (2021) Biotechnological trends and market impact on the recovery of rare earth elements from bauxite residue (red mud)- a review. Resour Conserv Recycl 171:105645. https://doi.org/10.1016/j.resconrec.2021.105645
33. Miao Q, Li M, Gao G, Zhang W, Zhang J, Yan B (2023) Improved process for separating TiO_2 from an oxalic-acid hydrothermal leachate of vanadium slag. Metals 13(20):1–20. https://doi.org/10.3390/met13010020
34. Li W, Wang N, Lu F, Chai H, Gu H (2023) Selective separation of aluminum, silicon, and titanium from red mud using oxalic acid leaching, iron precipitation and pH adjustments with calcium carbonate. Hydrometallurgy 223:106221. https://doi.org/10.1016/j.hydromet.2023.106221
35. Jha A, Cooke G, Lahiri A (2009) Process for recovering a titanium dioxide product, EP2329051A1 European patent office, 17–9, 2009.
36. Thambiliyagodage C, Wijesekera R, Bakker MG (2021) Leaching of ilmenite to produce titanium based materials: a review. Discov Mater 1:20. https://doi.org/10.1007/s43939-021-00020-0
37 de Oliveira ALB, da Silva GDS, de Aguiar PF, Afonso JC (2023) Optimization of alkaline roasting to enable acid leaching of titanium from anatase ores. Sustain Metall 9:183–193. https://doi.org/10.1007/s40831-022-00637-2
38. Ginting LI, Manaf A, Astuti W, Supriyatna YI, Bahfie F (2023) Study of titanium dioxide (TiO_2) extraction process from ilmenite Banten. IOP Conf Ser: Earth Environ Sci 1201:012092. https://doi.org/10.1088/1755-1315/1201/1/012092
39. LuévanosMartínez A, Rodriguez-Delgado MG, Uribe-Salas A, Carrillo-Pedroza FR, Osuna-Alarcón JG (2011) Leaching kinetics

of iron from low grade kaolin by oxalic acid solutions. Appl Clay Sci 51:473–477. https://doi.org/10.1016/j.clay.2011.01.011
40. Omidi MH, Nuri OS, Tavakoli H (2018) Optimization of ilmenite dissolution by synergistic effect of oxalic acid and hydrochloric acid for preparing synthetic rutile. Int J Nonferrous Metall 7:25–38
41. Jonglertjunya W, Rattanaphan S, Tipsak P (2014) Kinetics of the dissolution of ilmenite in oxalic and sulfuric acid solutions. Asia-Pac J Chem Eng 9:24–30. https://doi.org/10.1002/apj.1742
42. Nayl AA, Aly HF (2009) Acid leaching of ilmenite decomposed by KOH. Hydrometallurgy 97(1–2):86–93. https://doi.org/10.1016/j.hydromet.2009.01.011
43. Srivastava V, Werner J, Honaker R (2023) Design of multi-stage solvent extraction process for separation of rare earth elements. Mining 3:552–578. https://doi.org/10.3390/mining3030031
44. Innocenzi V, De Michelis I, Ferella F, Vegliò F (2017) Secondary yttrium from spent fluorescent lamps: recovery by leaching and solvent extraction. Int J Miner Process 168:87–94. https://doi.org/10.1016/j.minpro.2017.09.017
45. Abdellah WM (2020) Preparation of pure uranium, thorium, and yttrium oxides from El-Garra El-Hamra sulfate leach liquor. Radiochemistry 62:347–358. https://doi.org/10.1134/S1066362220030078
46. Abu Elgoud EM, Ismail ZH, El-Nadi YA, Aly HF (2020) Separation of cerium (IV) and yttrium (III) from citrate medium by solvent extraction using D_2EHPA in kerosene. Chem Pap 74:2461–2469. https://doi.org/10.1007/s11696-020-01083-8
47. Tunsu C, Lapp JB, Ekberg C, Retegan T (2016) Selective separation of yttrium and europium using Cyanex 572 for applications in fluorescent lamp waste processing. Hydrometallurgy 166:98–106. https://doi.org/10.1016/j.hydromet.2016.10.012
48. Jorjani E, Shahbazi M (2016) The production of rare earth elements group via tributyl phosphate extraction and precipitation stripping using oxalic acid. Arab J Chem 9(2):S1532–S1539. https://doi.org/10.1016/j.arabjc.2012.04.002
49. Li D (2017) A review on yttrium solvent extraction chemistry and separation process. J Rare Earths 35(2):107–119. https://doi.org/10.1016/S1002-0721(17)60888-3
50. Khalil M, El Hussaini O, Abd El Wahab G, Swafy S (2018) Chemical treatment of El Missikat fluorite-bearing ore material, Egypt, for recovery of pure yttrium oxide. Arab J Nucl Sci Appl 51(4):89–99. https://doi.org/10.21608/ajnsa.2018.12397
51. Marczenko Z (2000) Spectrophotometric determination of elements. John Wiley and Sons, Harwood, New York
52. Liu Y, Qi T, Chu J, Tong Q, Zhang Y (2006) Decomposition of ilmenite by concentrated KOH solution under atmospheric pressure. Int J Miner Process 81:79–84. https://doi.org/10.1016/j.minpro.2006.07.003
53 Kakihana M, Kobayashi M, Tomita K, Petrykin V (2010) Application of water-soluble titanium complexes as precursors for synthesis of titanium-containing oxides via aqueous solution processes. Bull Chem Soc Jpn 83(11):1285–1308. https://doi.org/10.1246/bcsj.20100103
54. Lee SO, Tran T, Jung BH, Kim SJ, Kim MJ (2007) Dissolution of iron oxide using oxalic acid. Hydrometallurgy 87:91–99. https://doi.org/10.1016/j.hydromet.2007.02.005
55. Jeng JM, Waches IS (1991) Niobium oxide solution chemistry. J Raman Spectrosc 22:83–89. https://doi.org/10.1002/jrs.1250220207
56. Amer TE, Abdellah WM, Abdel Wahab GM, El-Shahat MF (2017) Selective separation of yttrium and cerium (IV) from the prepared Abu Hamata lanthanides cake. Chem Biomol Eng 1(1):26–31. https://doi.org/10.11648/j.cbe.20160101.15